P12

AIAA 97-0143

Screech Tones of Supersonic Jets from Bevelled Rectangular Nozzles

Christopher K. W. Tam and Hao Shen
Florida State University
Tallahassee, FL

Ganesh Raman
NYMA Inc., Experimental Fluid Dynamics
NASA Lewis Research Center
Brook Park, OH

35th Aerospace Sciences Meeting & Exhibit
January 6-10, 1997 / Reno, NV

Screech Tones of Supersonic Jets from Bevelled Rectangular Nozzles†

Christopher K.W. Tam* and Hao Shen**
Florida State University
Tallahassee, FL 32306-3027

Ganesh Raman***
NYMA Inc., Experimental Fluid Dynamics Section
NASA Lewis Research Center
Brook Park, OH 44142

Abstract

It is known experimentally that an imperfectly expanded rectangular jet from a thin-lip convergent nozzle emits only a single dominant screech tone. The frequency of the screech tone decreases continuously with increase in jet Mach number. However, for a supersonic jet issued from a bevelled nozzle or a convergent-divergent nozzle with straight side walls, the shock cell structure and the screech frequency pattern are fairly complicated and have not been predicted before. In this paper, it is shown that the shock cell structures of these jets can be decomposed into waveguide modes of the jet flow. The screech frequencies are related to the higher-order waveguide modes following the weakest-link screech tone theory. The measured screech frequencies are found to compare well with the predicted screech frequency curves.

1. Introduction

Recently, there is a renewed interest in the possible application of rectangular jets to future generation aircraft propulsive system. Rectangular jets are regarded to have the potential for jet mixing enhancement and noise reduction. Furthermore, they are known to have thrust vectoring capability.

When operating at imperfectly expanded conditions, a supersonic rectangular jet emits discrete frequency screech tones. Earlier, these tones have been studied experimentally by Powell[1], Hammitt[2], Krothapalli *et al.*[3] and others. During the last few years, they are the subject of several research studies[4-10]. In the most recent work of Raman[10], bevelled rectangular nozzles were used. By shaping the nozzle exit geometry, it was hoped that there could be additional noise and mixing benefits.

The shock cell structure of an imperfectly expanded rectangular jet with a straight exit is quite complicated. Figure 1 shows the spark schlieren image of the top view of such a shock cell structure associated with an aspect ratio 5 convergent rectangular nozzle. The jet Mach number is 1.4. If, instead of a regular straight exit nozzle, a bevelled nozzle is used, the shock cell structure becomes even more complex. This can be seen in figure 2. The jet Mach number is again 1.4. The shock cell structure is not only highly three-dimensional but also contains many fine-scale features. However, overall the shock cell structure is still quasi-periodic.

It was observed experimentally, since the pioneering work of Powell[1], that a rectangular jet from a thin-lip convergent nozzle emits only one dominant screech tone (and its harmonics). Over the years, this finding has been confirmed by all subsequent investigators. Figure 3 shows a typical variation of the screech frequency with increase in jet Mach number. The data[10] is for a jet issued from an aspect ratio 5 convergent nozzle with exit dimensions 6.58 cm by 1.32 cm. In contrast to the simplicity of the regular straight nozzle case, the tone frequency Mach number relation for rectangular jets from bevelled nozzles, is highly complicated[10]. Observations revealed that it is possible for a jet to emit more than one dominant screech tones simultaneously. A closer inspection of the data indicates that even sudden frequency jumps can occur. At the present time, the physical mechanism responsible for this screech tone frequency pattern is not well understood.

The primary objective of the present investigation is to seek a physical explanation of the observed screech frequency jet Mach number relation for bevelled rectangular nozzles. Both convergent and convergent-divergent nozzles are considered. Obviously, the screech frequency must be closely related to the shock cell structure in the jet plume. For this

* Professor, Department of Mathematics, Associate Fellow AIAA.

** Graduate student, Department of Mathematics.

*** Senior Research Engineer, Member AIAA.

reason, a linear model shock cell structure of a supersonic jet from a bevelled rectangular nozzle will first be established. The use of a linear shock cell model for screech frequency and broadband shock associated noise prediction is not new. Such a model has been used successfully in ref. [11] to [15]. As in previous works, the present shock cell structure model is formed by a superposition of the waveguide modes of the jet flow. For screech frequency prediction, attention is focussed on the lower-order modes.

It is known[1,16] that screech tones are generated by a feedback loop. According to the weakest-link theory[17], the feedback loop is driven by the large-scale instability waves of the jet flow. The instability waves are excited at the nozzle exit region near the nozzle lip, where the jet is most receptive to external excitation, by acoustic disturbances. The excited instability waves extract energy from the mean flow and grow quickly as they propagate downstream. After propagating a distance of about three to four shock cells, they, having grown to relatively high amplitudes, interact strongly with the shock cell structure. As a result of the interaction, strong acoustic waves are generated. Part of the acoustic waves propagate upstream outside the jet. Upon impinging on the jet near the nozzle lip region, the acoustic disturbances excite the shear layer, thus generating new instability waves. In this way, the feedback loop is closed. Tam, Seiner and Yu[17] observed that the acoustic waves that radiated to the nozzle lip region were confined to a narrow frequency band if they were generated by the interaction between the large-scale instability waves and the quasi-periodic shock cell structure of a supersonic jet. The band is centered around frequency f_p given by,

$$f_p = \frac{u_c \kappa}{2\pi(1 + \frac{u_c}{a_\infty})} \tag{1}$$

where u_c is the convection or phase velocity of the instability waves. a_∞ is the ambient sound speed and κ is the wavenumber of the shock cell structure. The weakest link of the feedback loop is the process of excitation of the large-scale instability waves by the feedback acoustic waves near the nozzle lip. In order to maintain the loop, the screech tone frequency must fall within the narrow band centered around f_p given by (1). Because of this, equation (1) offers a good estimate of the screech frequency.

To be able to use (1) for screech frequency prediction, u_c and κ must first be found. For circular jets, Harper-Bourne and Fisher[18] had measured experimentally that $u_c \simeq 0.7u_j$ (u_j is the jet speed). However, for rectangular jets Tam and Reddy[19] found it was more appropriate to use a lower convection velocity. They recommended

$$u_c \simeq 0.55u_j. \tag{2}$$

In this work, formula (2) will be used throughout.

By means of a vortex sheet jet model, Tam[12] found that the pressure distribution, p, associated with the shock cell structure of a rectangular jet can be decomposed into waveguide modes with eigenfunctions (mode shape), $\phi_{nm}(y,z)$ and wavenumber k_{nm}. With respect to a Cartesian coordinate system shown in figure 4 for a jet with fully expanded width b_j and height h_j, p may be represented by an expansion in the form

$$p(x,y,z) = \sum_{n=1}^{\infty}\sum_{m=1}^{\infty} \phi_{nm}(y,z)[A_{nm}\cos(k_{nm}x) + B_{nm}\sin(k_{nm}x)] \tag{3}$$

where

$$\phi_{nm}(y,z) = \sin\left(\frac{n\pi y}{b_j}\right)\sin\left(\frac{m\pi z}{h_j}\right) \tag{4}$$

$$k_{nm} = \left(\frac{n^2}{b_j^2} + \frac{m^2}{h_j^2}\right)^{\frac{1}{2}} \frac{\pi}{(M_j^2-1)^{\frac{1}{2}}}. \tag{5}$$

The coefficients A_{nm} and B_{nm} are to be determined by the nozzle exit conditions. b_j and h_j are related to the nozzle exit dimensions, b and h, by

$$\frac{b_j}{b} = \left(\frac{A_j}{hb} - 1\right)\left(\frac{h}{h+b}\right) + 1 \tag{6}$$

$$\frac{h_j}{h} = \left(\frac{A_j}{bh} - 1\right)\left(\frac{b}{b+h}\right) + 1 \tag{7}$$

where

$$\frac{A_j}{bh} = \frac{M_d}{M_j}\left(\frac{1+\frac{\gamma-1}{2}M_j^2}{1+\frac{\gamma-1}{2}M_d^2}\right)^{\frac{\gamma+1}{2(\gamma-1)}}. \tag{8}$$

In the above, M_j is the fully expanded jet Mach number and M_d is the nozzle design Mach number.

For shock cell mode prediction, the linear model above is fairly accurate. For instance, the screech frequency of the measured data in figure 3 can be predicted by taking κ in formula (1) to be the wavenumber of the lowest waveguide mode ($n = 1$, $m = 1$); i.e.,

$$\kappa = k_{11} = \left(\frac{1}{b_j^2} + \frac{1}{h_j^2}\right)^{\frac{1}{2}} \frac{\pi}{(M_j^2-1)^{\frac{1}{2}}}. \tag{9}$$

The calculated values form the solid curve of this figure. As can be seen, there is good agreement between the measured data and the theoretical prediction over a wide range of Mach numbers.

For bevelled rectangular nozzles, the associated shock cells are necessarily more complicated. For the stated purpose of this investigation, namely, to obtain a physical understanding of the screech frequency pattern of these jets, it is believed that the use of a linear shock cell model is sufficient. The development of such a model will be discussed below. The results of the model is then used in section 3 of this paper to predict the screech tone frequency jet Mach number relation. Comparisons with experimental measurements are carried out. The experimental measurements involved jets from single bevelled nozzles, double bevelled nozzles and regular nozzles. Both convergent and convergent-divergent nozzles are included.

2. The Shock Cell Structure and Screech Frequencies

2.1 The Physical Model

Let us consider the shock cell structure of a rectangular jet from a single bevelled rectangular nozzle. Figure 5 shows the plan view of such a jet. For simplicity, we will use a vortex sheet jet model as in the work of Tam[12]. We will assume that the jet Mach number M_j is such that the bevelled angle β is larger than the Mach angle μ. When this is true the disturbances generated by the upstream nozzle side wall would not reach the inside of the nozzle. That is, all the flow disturbances produced by the boundary discontinuities at the nozzle exit are confined within the jet flow.

For weak shock cells, the shock structure disturbances are governed by the linearized equations of motion. On following Tam[12], it is straightforward to find that the pressure, p, of the shock cells satisfies the equation

$$\nabla^2 p - M_j^2 \frac{\partial^2 p}{\partial x^2} = 0. \tag{10}$$

On the boundaries of the jet (see figure 5) the pressure balance boundary condition across the vortex sheet must be satisfied. That is, at $y = 0$, $y = b_j$, $z = 0$, $z = h_j$

$$p = 0. \tag{11}$$

At the nozzle exit, $y = -x \tan\beta$, both p and $\frac{\partial p}{\partial x}$ are prescribed. These are the initial conditions determined by the supersonic flow upstream (inside the nozzle). For a convergent nozzle, a simple model of the initial conditions is,

$$p = \Delta p \quad \text{(constant)} \tag{12}$$

$$\frac{\partial p}{\partial x} = 0. \tag{13}$$

For convergent-divergent nozzles with straight side walls, Tam and Reddy[19] have pointed out that a second set of shock cells would be generated at the nozzle throat. Thus the pressure distribution at the nozzle exit cannot be constant. Therefore, (12) and (13) would not be appropriate for these types of nozzles.

2.2 Numerical Solution

Initial boundary value problem (10) to (13) can be solved relatively easily if the solution is first expanded as a Fourier series in z. That is, let

$$p(x, y, z) = \sum_{m=1}^{\infty} \hat{p}_m(x, y) \sin\left(\frac{m\pi z}{h_j}\right). \tag{14}$$

On substitution of (14) into (10), the governing equation for $\hat{p}_m(x, y)$ is found to be,

$$(M_j^2 - 1)\frac{\partial^2 \hat{p}_m}{\partial x^2} - \frac{\partial^2 \hat{p}_m}{\partial y^2} + \frac{m^2\pi^2}{h_j^2}\hat{p}_m = 0. \tag{15}$$

The boundary conditions from (11) are, at $y = 0$, $y = b_j$

$$\hat{p}_m = 0. \tag{16}$$

On expanding (12) and (13) in Fourier series of $\sin(\frac{m\pi z}{h_j})$, it is straightforward to find that the initial conditions at the nozzle exit, $y = -x \tan\beta$, are

$$\hat{p}_m = \frac{2}{m\pi}(1 - \cos m\pi)\Delta p \tag{17}$$

$$\frac{\partial \hat{p}_m}{\partial x} = 0. \tag{18}$$

We solve equation (15), boundary condition (16) and initial conditions (17) and (18) by finite difference method. To keep the order of the finite difference equations the same as the order of the original partial differential equation (15), we choose to approximate the spatial derivatives by second-order central differences. One principal reason for using a second order finite difference approximation instead of a higher-order scheme is that the number of initial and boundary conditions for the resulting finite difference equation is identical to those of the original partial differential equation problem. Had a higher-order scheme been used, extra initial and boundary conditions must be imposed in order to

obtain a unique solution. Then a way must be found to impose these extra conditions so that they have no effect on the numerical results. With respect to a mesh of spacing Δx and Δy as shown in figure 6, the discretized form of (15) is,

$$(M_j^2-1)\frac{(\hat{p}_{\ell+1,k}-2\hat{p}_{\ell,k}+\hat{p}_{\ell-1,k})}{\Delta x^2} - \frac{(\hat{p}_{\ell,k+1}-2\hat{p}_{\ell,k}+\hat{p}_{\ell,k-1})}{\Delta y^2} + \frac{m^2\pi^2}{h_j^2}\hat{p}_{\ell,k}=0 \tag{19}$$

where (ℓ, k) are the mesh indices in the x- and y-directions. (19) may be rewritten in the following form so that the value of $\hat{p}_{\ell+1,k}$ may be computed once its values at the last two columns, ℓ and $\ell-1$, are known.

$$\hat{p}_{\ell+1,k}=\left(\frac{\Delta x}{\Delta y}\right)^2\frac{1}{M_j^2-1}(\hat{p}_{\ell,k+1}+\hat{p}_{\ell,k-1}) + \left(2-\frac{m^2\pi^2}{h_j^2}\frac{(\Delta x)^2}{M_j^2-1} - 2\left(\frac{\Delta x}{\Delta y}\right)^2\frac{1}{M_j^2-1}\right)\hat{p}_{\ell,k}-\hat{p}_{\ell-1,k}. \tag{20}$$

Suppose $\Delta y=\frac{b_j}{K}$ where K is a large integer. Then (20) is valid for $1\le k\le K-1$.

Boundary conditions (16) yield,

$$\hat{p}_{\ell,0}=\hat{p}_{\ell,K}=0. \tag{21}$$

To ensure that the computed solution satisfies initial conditions (17) and (18) at the nozzle exit, a simple way is to start calculating the solution using (20) at the column AA' ($\ell=-N$) as shown in figure 6. We set

$$\hat{p}_{-N,k}=\hat{p}_{-(N+1),k}=\frac{2}{m\pi}(1-\cos m\pi)\Delta p \tag{22}$$

and use (20) to march the solution in the x-direction. As soon as the value of $\hat{p}_{\ell,k}$ at a new ℓ column (at the first step, this will be $\ell=-N+1$) is found all the values of $\hat{p}_{\ell,k}$ at mesh points that lie inside the nozzle are reset to $\frac{2}{m\pi}(1-\cos\pi)\Delta p$. This assures that at the nozzle exit the slope in the x-direction is zero and also the pressure there is equal to the right side of (17). The marching process is to be continued until $\ell>0$ is reached.

Finite difference equation (20) is computationally unstable unless a small value of Δx is used. The stability requirement of (20) can be established by performing a standard Von Neumann analysis. Let

$$\hat{p}_{\ell,k}=\sigma^\ell e^{i\lambda k}. \tag{23}$$

Substitution of (23) into (20) leads to the following equation for σ.

$$\sigma^2-Q\sigma+1=0 \tag{24}$$

where

$$Q=\left(\frac{\Delta x}{\Delta y}\right)^2\frac{2}{M_j^2-1}(\cos\lambda-1) + 2-\frac{m^2\pi^2}{h_j^2}\frac{(\Delta x)^2}{M_j^2-1}. \tag{25}$$

The roots of (24) are

$$\sigma_\pm=\frac{1}{2}[Q\pm(Q^2-4)^{\frac{1}{2}}]. \tag{26}$$

One of the roots of (26) will have a magnitude greater than unity unless $\sigma_\pm$ are complex conjugates of each other in which case $|\sigma_\pm|=1$. The computation scheme is, therefore, stable if $Q^2<4$. This yields

$$-4<\left(\frac{\Delta x}{\Delta y}\right)^2\frac{2}{M_j^2-1}(\cos\lambda-1) - \frac{m^2\pi^2}{k_j^2}\frac{(\Delta x)^2}{M_j^2-1}<0. \tag{27}$$

The right side inequality of (27) is always satisfied. The left side inequality would be satisfied for all λ provided,

$$\left(\frac{\Delta x}{\Delta y}\right)^2\frac{4}{M_j^2-1}+\frac{m^2\pi^2}{h_j^2}\frac{(\Delta x)^2}{M_j^2-1}<4.$$

Thus, numerical stability is assured if Δx is taken to be

$$\Delta x<\frac{(M_j^2-1)^{\frac{1}{2}}\Delta y}{[1+\frac{m^2\pi^2}{4}(\frac{\Delta y}{h_j})^2]^{\frac{1}{2}}}. \tag{28}$$

In the present numerical computation, the step size Δx used is always smaller than that given by the right side of (28).

2.3 Waveguide Modes of the Shock Cell Structure

In the region of the jet downstream of the y-axis at $\ell=0$, the shock cell solution can again be expanded in terms of the waveguide modes of the jet

flow as in equation (3). In this case $\widehat{p}_m(x,y)$ may be written in the form,

$$\widehat{p}_m(x,y) = \sum_{n=1}^{\infty} \sin\left(\frac{n\pi y}{b_j}\right)[A_{nm}\cos(k_{nm}x) + B_{nm}\sin(k_{nm}x)]. \quad (29)$$

The coefficients A_{nm} and B_{nm} are to be determined by joining expansion (29) smoothly to the numerical solution at a location, say, at $\ell = L$ $(L > 0)$. The joining conditions are the continuity of $\widehat{p}_m$ and $\frac{\partial \widehat{p}_m}{\partial x}$. On replacing integrals by appropriate sums (the numerical solution is in discretized form), it is straightforward to find from the joining conditions that the values of A_{nm} and B_{nm} are given by,

$$A_{nm} = \frac{2\Delta y}{k_{nm}b_j}\left[k_{nm}\cos(k_{nm}L\Delta x)\sum_{k=0}^{K}\widehat{p}_{L,k} \cdot \sin\left(\frac{n\pi k\Delta y}{b_j}\right) - \sin(k_{nm}L\Delta x) \cdot \sum_{k=0}^{K}\frac{1}{2\Delta x}(\widehat{p}_{L+1,k} - \widehat{p}_{L-1,k}) \cdot \sin\left(\frac{n\pi k\Delta y}{b_j}\right)\right] \quad (30)$$

$$B_{nm} = \frac{2\Delta y}{k_{nm}b_j}\left[k_{nm}\sin(k_{nm}L\Delta x)\sum_{k=0}^{K}\widehat{p}_{L,k} \cdot \sin\left(\frac{n\pi k\Delta y}{b_j}\right) + \cos(k_{nm}L\Delta x) \cdot \sum_{k=0}^{K}\frac{1}{2\Delta x}(\widehat{p}_{L+1,k} - \widehat{p}_{L-1,k}) \cdot \sin\left(\frac{n\pi k\Delta y}{b_j}\right)\right]. \quad (31)$$

The amplitude of the (m,n) waveguide mode is

$$C_{nm} = (A_{nm}^2 + B_{nm}^2)^{\frac{1}{2}}. \quad (32)$$

2.4 Screech Frequencies

Beyond the most downstream edge of the nozzle, the shock cell structure is quasi-periodic. This is the region where the feedback acoustic waves of the screech feedback loop are generated. The physical situation is very similar to that of a jet with a regular straight nozzle exit. The major difference lies in that the dominant waveguide modes that make up the quasi-periodic shock cell structure are not necessarily the lowest order modes. Moreover, it is possible that more than one mode is dominant. As far as the screech tone feedback loop is concerned, the weakest-link theory is still applicable. However, we expect the resulting screech tones to be more complex. This is because they are related to the higher-order modes as well as more than one feedback loop may be operating at the same time. On following Tam[12], the screech frequencies can be calculated by replacing κ in equation (1) by k_{nm} given by equation (5). For a large aspect ratio jet $(b_j >> h_j)$ only the $m = 1$ modes are relevant. On restricting our consideration to the $m = 1$ modes, we obtain,

$$f_n = \frac{0.55u_j}{2\pi(1+\frac{0.55u_j}{a_\infty})}\left(\frac{n^2}{b_j^2} + \frac{1}{h_j^2}\right)^{\frac{1}{2}}\frac{\pi}{(M_j^2-1)^{\frac{1}{2}}} \quad (33)$$

$n = 1, 2, 3, \ldots$.

3. Comparisons with Experiments

Detailed variations of the screech tone frequencies with jet Mach number for an aspect ratio 5 jet have been measured by Raman[10]. In this section, we will compare the frequencies of his measured data with formula (33).

In the experiments of Raman, six rectangular nozzles were used. Three were convergent nozzles and the other three were C-D nozzles. In each family of nozzles, one has a regular straight exit geometry, the second has a single-bevelled and the third a double-bevelled geometry. The dimensions of these nozzles were given in the works of Rice and Raman[5,6]. The variation of the screech tone frequencies with fully expanded jet Mach number for each nozzle was measured. However, because more effort was spent on the C-D nozzles, only data related to them were reported. In addition to screech frequencies, the spanwise phase difference and transverse phase difference of the screech tones were also measured. According to the phase information, Raman was able to separate the screech tones into different modes.

Figure 7 shows the measured screech tone frequencies as a function of the jet Mach number for the supersonic jet from the single-bevelled convergent rectangular nozzle. The data does not seem to form a continuous curve. There are frequency jumps at several jet Mach number. Shown also in this figure are the screech frequencies of formula (33) with spanwise mode number $n = 1, 2, 3$, and 4. As can be seen, the data correlate well with the theoretical frequency curves over the entire range of measured Mach numbers. Figure 8 shows a comparison of the

measured screech frequency and the frequencies of formula (33) for rectangular jets from the double-bevelled convergent nozzle. The screech frequencies agree well with the $n = 5$ and $n = 6$ frequency curves.

Figure 9 shows the variation of the screech frequency with Mach number for the supersonic jet from the C-D rectangular nozzle with a regular exit geometry. Based on his spanwise phase data, Raman was able to identify three distinct screech modes. Their frequencies fit very well with the frequencies of the $n = 1, 3$ and 5 modes of formula (33). Figure 10 provides the measured screech frequency jet Mach number relation of the supersonic jet from the single-bevelled C-D rectangular nozzle. According to the phase data, there are three modes, i.e., mode I, modes IIIA and IIIB. Shown also are the screech frequency curves for $n = 1, 2, 3$ and 4 modes according to formula (33). The data appear to agree well with the frequency curves of the $n = 1, 2$ and 4 modes. Finally, figure 8 shows the measured screech frequency variation with jet Mach number of the supersonic jet from the C-D double-bevelled rectangular nozzle. Two modes have been identified. Their frequencies are in reasonable agreement with the $n = 6$ and $n = 7$ frequency curves of formula (33).

Formula (33) predicts many screech frequency bands. However, not all the tones of the frequency bands are excited. We believe that the selection of the excited frequencies is determined largely by two factors. They are the spatial growth rates of the instability waves of the jet flow and the strength of the waveguide modes of the shock cell structure. Here, we will examine, by means of the shock cell model above, how the strength of the waveguide modes influences tone selection as well as the frequency jumps in the data of figure 7. For this purpose, the amplitudes of the waveguide modes corresponding to $m = 1$, $n = 1, 2, 3, 4$ were calculated by the marching scheme (20). In the numerical computation K was taken to be 8000. The size of the marching step Δx was chosen to be smaller than that given by (28). The solution was marched from the starting line AA' in figure 6 to a line downstream of the y-axis before the coefficients A_{n1}, B_{n1} and C_{n1} were evaluated according to equations (30) to (32). To check the accuracy of the numerical results, each computation was marched further downstream. At this new location, the amplitude C_{n1} was again determined. It was found in every case that the two calculated values of C_{n1} agreed to, at least, three significant figures. This offers assurance that the numerical results are accurate.

Figure 12 shows the computed waveguide mode amplitude C_{n1}, $n = 1, 2, 3, 4$ of the shock cell structure for a single bevelled convergent rectangular nozzle used in the experiment of Raman[10]. In the computation, Δp was set equal to unity for convenience. At low supersonic Mach number, the dominant mode is the $n = 4$ mode. As the Mach number increases, the dominant mode shifts to $n = 3$, then $n = 2$, and finally at $M_j > 2$ the $n = 1$ mode becomes the most dominant. This trend correlates well with the measured data in figure 7.

If the shock cell strength is the only factor that determines the dominant screech tone, then the information in figure 8 can be used to predict the locations of the frequency jumps observed in figure 7. Let us assume that a shift in the excited frequency is possible when the waveguide mode amplitude of the adjacent band is within 15% of each other. Figure 13 shows the mode switching Mach number or the expected locations of frequency jumps. The predicted locations for mode switching from $n = 4$ to $n = 3$ and from $n = 3$ to $n = 2$ (indicated by arrows) are in fair agreement with measurements. The switch from $n = 2$ to $n = 1$ mode takes place around $M_j = 1.75$ whereas the calculated value falls around $M_j = 2.0$. We believe that the discrepancy is solely because the effect of the growth rate of the instability waves has not been taken into account. Despite this discrepancy, the good overall agreement leaves little doubt that the strength of the waveguide modes of the shock cell structure plays a crucial role in the selection of the observed screech tones.

4. Summary and Discussion

The screech tone frequency patterns of supersonic jets from bevelled rectangular nozzles and C-D nozzles with straight side walls are quite complex. In this paper, it is suggested that these tones are related to the higher order waveguide modes of the shock cell structure in the jet plume. By using a simple vortex sheet jet model to calculate the linear shock cell waveguide modes of the jet and then calculate the screech frequencies by the axial wavenumber of these modes, it is shown that the predicted screech frequency curves agree well with all the measured data. The good agreement provides strong support for the waveguide mode concept of the shock cell structure and the weakest-link feedback theory of jet screech.

In the present work, the shock cell structure is modelled by a superposition of waveguide modes of the jet flow. This modal decomposition is unquestionably at odds with the concept of shock cells

with sharp discontinuities. One major difference between the two models is that there can only be one screech tone associated with a shock cell structure with sharp discontinuities (there is only one shock cell length). On the other hand, there can be more than one screech tone according to the waveguide model. In the above, we have found good agreements between the screech frequencies predicted by the waveguide shock cell model and experimental measurements. Furthermore, Raman[10] has shown experimentally that two screech tones can exist simultaneously. Thus there is no question that a waveguide model representation of the shock cells of a supersonic jet is valid. However, the authors believe that the range of validity is limited only to the moderately imperfectly expanded Mach number range of the nozzle. For highly imperfectly expanded jets, nonlinear effects dominate the formation of the shock cell structure. In this case, the structure is made up of sharp shocks. It follows, therefore, for highly imperfectly expanded jets there would only be a single screech tone. This appears to be consistent with all the screech tone data available in the literature at the present time.

Acknowledgment

The work of CKWT and HS was supported in part by NASA Langley Research Center Grant NAG 1-1776.

References

1. Powell, A., "On the Noise Emanating from a Two-Dimensional Jet above the Critical Pressure," Aeronautical Quarterly, vol. 4, 1953, pp 103–122.
2. Hammitt, A.G., "The Oscillation and Noise of an Overpressure Sonic Jet," Journal of Aerospace Sciences, vol. 28, 1961, pp 673–680.
3. Krothapalli, A., Hsia, Y., Baganoff, D. and Karamcheti, K., "The Role of Screech Tones on Mixing of an Underexpanded Rectangular Jet," Journal of Sound and Vibration, vol. 106, 1986, pp. 119–143.
4. Rice, E.J. and Taghavi, R., "Screech Noise Source Structure of a Supersonic Rectangular Jet," AIAA Paper 92-0503, 1992.
5. Rice, E.J. and Raman, G., "Mixing Noise Reduction for Rectangular Supersonic Jets by Nozzle Shaping and Induced Screech Mixings," AIAA Paper 93-4322.
6. Rice, E.J. and Raman, G., "Supersonic Jets from Bevelled Rectangular Nozzles," ASME Paper 93-WA/NCA-26.
7. Raman, G. and Rice, E.J., "Instability Modes Excited by Natural Screech Tones in a Supersonic Rectangular Jet," Physics of Fluids, vol. 6, Dec. 1994, pp. 3999–4008.
8. Umeda, Y. and Ishii, R., "Oscillation Modes of Underexpanded Jets Issuing from Square and Equilateral Triangular Nozzles," Journal of Acoustical Society of America, vol. 95, 1994, pp. 1853–1857.
9. Walker, S.H., Gordeyer, S.V. and Thomas, F.O., "A Wavelet Transform Analysis Applied to Unsteady Jet Screech Resonance," Proceedings ASME/JSME Fluids Engineering and Laser Anemonetry Conference and Exhibition, Hilton Head, SC, Aug. 1995, pp. 103–108.
10. Raman, G., "Screech Tones from Rectangular Jets with Spanwise Oblique Shock-Cell Structures," AIAA Paper 96-0643, Jan 1996.
11. Tam, C.K.W., Jackson, J.A. and Seiner, J.M., "A Multiple-Scales Model of the Shock Cell Structure of Imperfectly Expanded Supersonic Jets," J. Fluid Mech., vol. 153, 1985, pp 123–149.
12. Tam, C.K.W., "The Shock-Cell Structure and Screech Tone Frequencies of Rectangular and Non-Axisymmetric Supersonic Jets," Journal Sound & Vibration, vol. 121, 1988, pp 135–147.
13. Morris, P.J., Bhat, T.R.S. and Chen, G., "A Linear Shock Cell Model for Jets of Arbitrary Exit Geometry," Journal Sound Vibration, vol. 132, 1989, pp. 199–211.
14. Tam, C.K.W., "Broadband Shock Associated Noise of Moderately Imperfectly Expanded Supersonic Jets," J. Sound and Vibration, 140, 1988, pp. 55-71.
15. Tam, C.K.W., "Broadband Shock Associated Noise from Supersonic Jets Measured by a Ground Observer," AIAA J., 30, Oct. 1992, pp. 2395–2401.
16. Tam, C.K.W., "Supersonic Jet Noise," Annual Review of Fluid Mechanics, 27, 1995, pp. 17–43.
17. Tam, C.K.W., Seiner, J.M. and Yu, J.C., "Proposed Relationship between Broadband Shock Associated Noise and Screech Tones," J. Sound & Vibration, vol. 110, 1986, pp 309–321.
18. Harper-Bourne, M. and Fisher, M.J., "The Noise from Shock Waves in Supersonic Jets," Proceedings (no. 131) of the AGARD Conference on Noise Mechanisms, 1973, Brussels, Belgium.
19. Tam, C.K.W. and Reddy, N.N., "Prediction Method for Broadband Shock Associated Noise from Supersonic Rectangular Jets," J. Aircraft, vol. 33, Mar-Apr 1996, pp. 298–303.

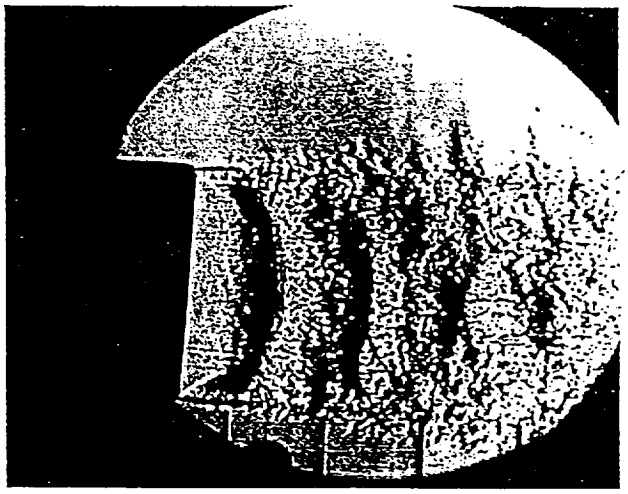

Figure 1 Spark schlieren image of the shock cell structure of a Mach 1.4, aspect ratio 5, rectangular jet from a regular convergent nozzle

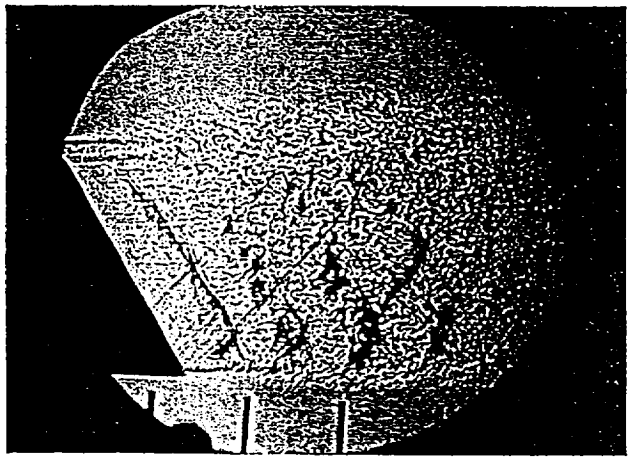

Figure 2 Spark schlieren image of the shock cell structure of a Mach 1.4, aspect ratio 5, rectangular jet from a single bevelled convergent nozzle

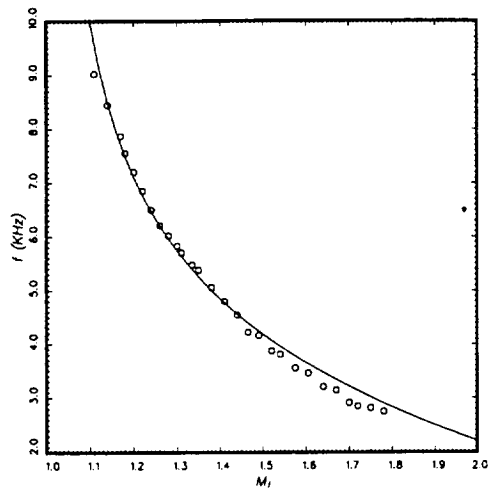

Figure 3 Variation of the screech frequency with fully expanded jet Mach number for a supersonic jet from a convergent rectangular nozzle. Aspect ratio = 5. Exit geometry = regular. O measurements[10]; —— theory[12].

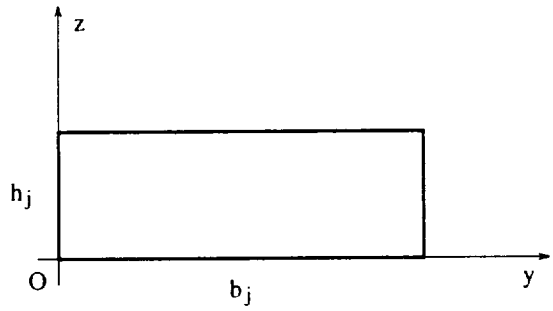

Figure 4 Coordinates used to calculate the shock cell structure of rectangular jets.

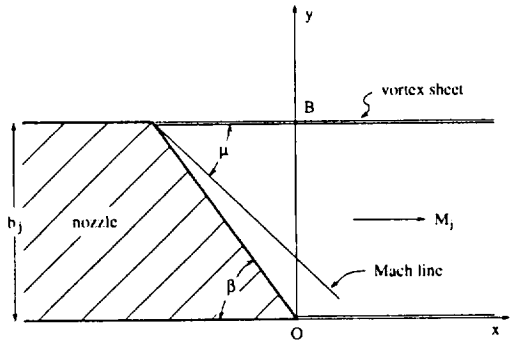

Figure 5 Top view of a vortex sheet jet from a single bevelled rectangular nozzle.

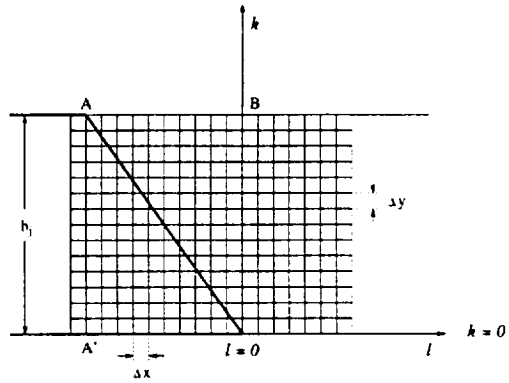

Figure 6 The computation domain with mesh size Δx and Δy .

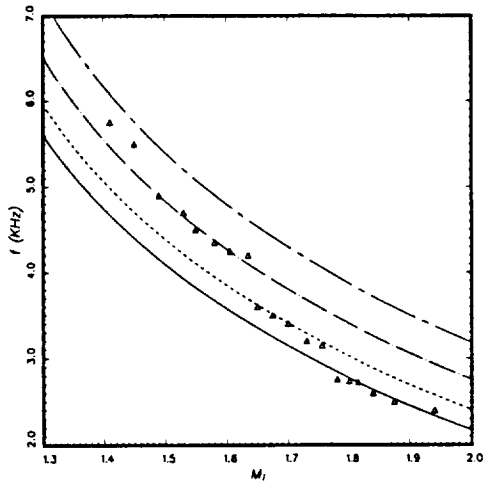

Figure 7 Variation of the screech frequencies with fully expanded jet Mach number for a supersonic jet from a convergent rectangular nozzle. Aspect ratio = 5. Exit geometry = single bevelled. Δ measurements[10]. Equation (33); —— n=1. - - - n=2, — · — n=3, — - — n=4.

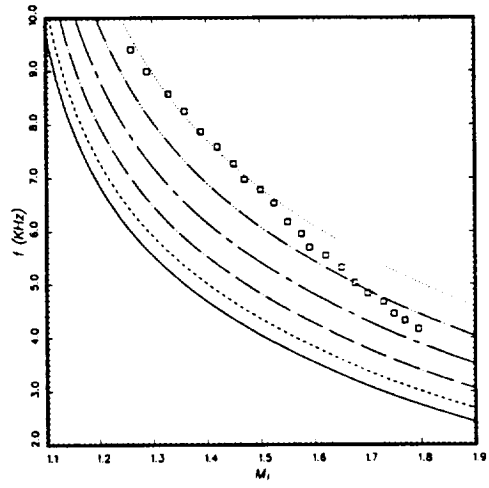

Figure 8 Variation of the screech frequencies with fully expanded jet Mach number for a supersonic jet from a convergent rectangular nozzle. Aspect ratio = 5. Exit geometry = double bevelled. □ measurements[10]. Equation (33); —— n=1, - - - n=2, — · — n=3, — - — n=4, — ·· — n=5, ····· n=6.

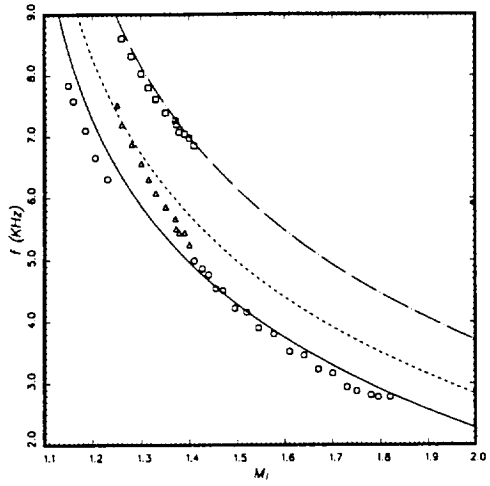

Figure 9 Variation of the screech frequencies with fully expanded jet Mach number for a supersonic jet from a convergent-divergent rectangular nozzle. Aspect ratio = 5. M_d = 1.4. Exit geometry = regular. Measurements[10]: ○ mode I-1, △ mode I-2, □ mode II . Equation(33); —— n=1, - - - n=3, — · — n=5.

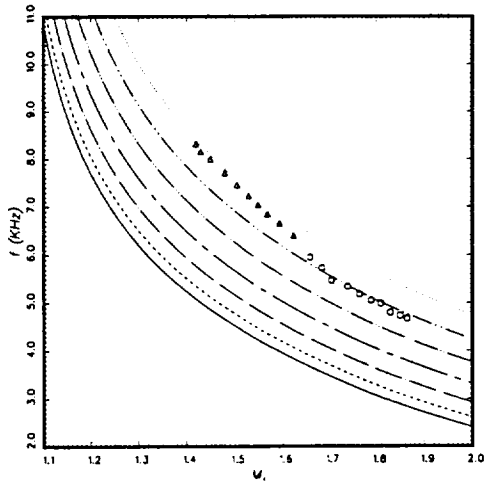

Figure 11 Variation of the screech frequencies with fully expanded jet Mach number for a supersonic jet from a convergent-divergent rectangular nozzle. Aspect ratio = 5. Exit geometry = double bevelled. Measurements[10]: ○ mode I. △ mode II. Equation(33): — - - — n=6, · · · · · n=7.

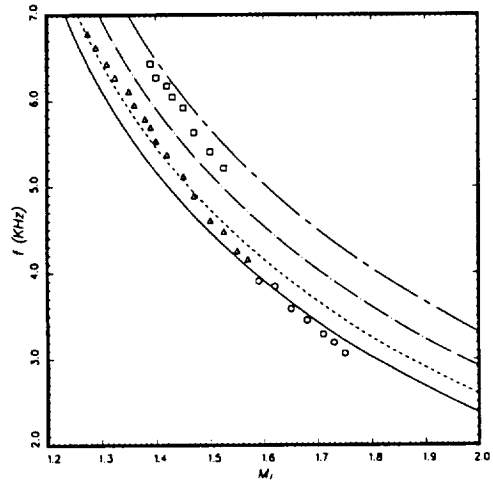

Figure 10 Variation of the screech frequencies with fully expanded jet Mach number for a supersonic jet from a convergent-divergent rectangular nozzle. Aspect ratio = 5. M_d = 1.4. Exit geometry = single bevelled. Measurements[10]: ○ mode I, △ mode III-A, □ mode III-B . Equation(33); —— n=1, - - - n=2, — · — n=3, — - — n=4.

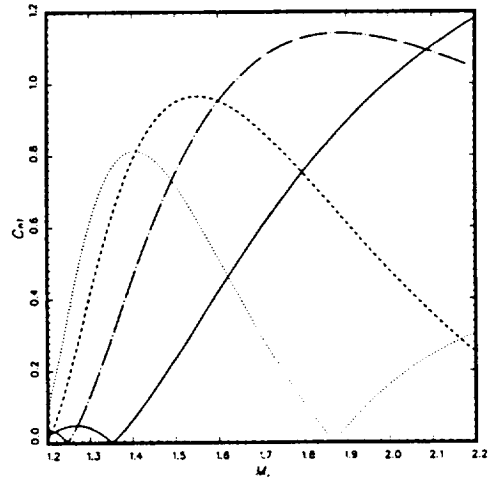

Figure 12 The amplitude of the waveguide modes of the shock cell structure in the plume of a supersonic jet downstream of a convergent single bevelled rectangular nozzle. Aspect ratio = 5. C_{11} ——, C_{21} — · —, C_{31} - - - -, C_{41} · · · · · · · ·.

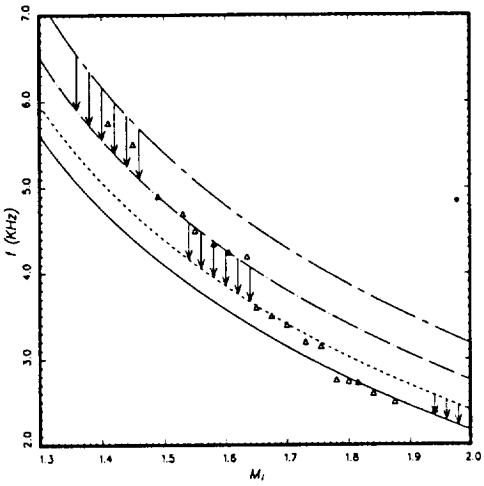

Figure 13 Mode-switching Mach numbers. ↓↓↓↓ based on computed waveguide mode amplitudes.